Statistical calculations of nuclear fragment distributions

Scott Pratt and Subal Das Gupta*
Department of Physics and Astronomy and National Superconducting Cyclotron Laboratory, Michigan State University, East Lansing, Michigan 48824

(Received 2 March 1999; revised manuscript received 18 January 2000; published 1 September 2000)

The recursive techniques developed by Mekjian and collaborators for exact calculations of canonical partition functions of fragmenting systems are extended to allow the determination of fragment multiplicity distributions. The fragment multiplicity distribution is shown to become strongly super-Poissonian at the critical temperature. This behavior is shown to be highly sensitive to Coulomb effects and to whether energy is strictly conserved (the microcanonical ensemble). Additionally, a method is presented for generating events from the partition functions, which also permits the inclusion of hard-sphere interactions between fragments.

PACS number(s): 25.70.Pq, 24.10.Pa, 64.60.My

I. INTRODUCTION

Heavy ion collisions where excitation energies are of the order of 10 MeV per nucleon probe the energy regime where the nuclear liquid gas transition is expected to take place. Below energies of approximately 50*A* MeV, symmetric collisions are expected to produce sources that evaporate particles as would be expected from a hot liquid drop, whereas above this threshold, the excited source is expected to explode, producing larger clusters through simultaneous multifragmentation. In this energy regime, the process of fragment production is not clear, and comparisons with data have been made with a disparate set of models, ranging in simplicity from percolation descriptions [1,2] and lattice gas models [3], to evaporative models [4], dynamical simulations [5–9], and microcanonical samplings [11–13].

Fluctuations behave in a special manner in the neighborhood of a phase transition, so it should seem that the study of fluctuations of fragmentation observables might prove insightful for investigating multifragmentation. Moretto and collaborators [14] have measured multiplicity distributions of intermediate-mass fragments (IMFs) as a function of excitation energy for a variety of projectile/target combinations utilizing beams with energies up to 60*A* MeV. The analysis showed sub-Poissonian multiplicity distributions that could accurately be described with binomial distributions. These observations have inspired a variety of explanations [15–18].

Recently, Chase and Mekjian [19] have discovered a method for exact calculation of the canonical partition function for noninteracting clusters. In this paper we extend this approach to include fragmentation observables. We present a method for exact determination of both multiplicity distributions and their moments for both canonical and microcanonical treatments. The canonical ensemble is appropriate for a system in contact with a large heat bath, while microcanonical descriptions are valid for a system with a fixed energy.

When raising the temperature while keeping the volume fixed in a canonical treatment, we observe a sharp transition for fragmentation at the same temperature where the specific heat peaks. At this threshold, the multiplicity distribution becomes remarkably wide. We associate this behavior with a first order phase transition. We find no such dramatic behavior for microcanonical calculations when plotted against the excitation energy. But, nonetheless the character of the multiplicity distributions does indeed change at the fragmentation threshold.

We also present a technique for generating random events consistent with the exact partition functions. By excluding those events where fragments overlap, we explicitly incorporate hard-sphere repulsion between fragments, and find that excluded volume arguments well account for the hard-sphere repulsions.

The status of statistical treatments of nuclear multifragmentation is reviewed in the next section. The correlation coefficient ξ, with which we parametrize the width of the fragment multiplicity distribution, is described in the third section. The methods for calculating partition functions and multiplicity distributions, and for generating random events is described in Sec. IV. Results and conclusions are presented in Secs. V and VI, respectively.

II. STATISTICAL MODELS OF MULTIFRAGMENTATION

The challenge of handling statistics of a finite-sized system that could fragment into arbitrary pieces has received great attention from the nuclear physics community during the last 20 years. Fragment yields were first calculated with grand canonical ensembles [10], which assume contact with both a heat bath and a particle reservoir. This approach is simple to implement and should accurately calculate single-particle yields in the limit of large systems where the size is not appreciably altered by the creation of a single fragment.

The finite system suggests that canonical and microcanonical treatments should be more appropriate. Koonin and Randrup [11] first developed a microcanonical treatment based on Metropolis Monte Carlo methods. A microcanonical approach was further pursued by Gross and collaborators and is referred to as MMMC (microcanonical statistical multifragmentation model) [12]. A large number of comparisons to experimental observables have been performed with this model, including a study of the binomial nature of the frag-

*Permanent address: Physics Department, McGill University, Montreal, Quebec, Canada H3A 2T8.

ment multiplicity distributions. The method consists of sampling fissions and fusions of nuclear fragments within a fixed volume. Energy, charge, and baryon number are divided amongst the various degrees of freedom. The advantage of this approach is that *N*-body correlations and explicit *N*-body interactions may be considered without computational penalty. The only disadvantage to this treatment is that computational requirements can be high, especially when fluctuations are of explicit interest and the event-to-event correlations of the Metropolis method must be eliminated.

Bondorf and collaborators [13] developed an alternative statistical treatment SMM (statistical multifragmentation model), where all possible partitions of the system into fragments are considered without invoking a Monte Carlo procedure. However, division of the energy between the internal and kinetic energy of the fragments does require Monte Carlo methods. Since in SMM the internal excitation energy is divided up amongst the fragments in proportion to the fragment mass, fluctuations of excitation energy are not treated as one would expect in a true microcanonical treatment. Furthermore, explicit *N*-body correlations and interactions are ignored.

A third approach invented by Mekjian [19,20] allows the calculation of statistical partition functions using recursion relations without invoking Monte Carlo methods. An approximate approach, also invoking an iterative procedure, was developed by Fai and Randrup [21]. The advantage of Mekjian's approach is that all partitions of the system are considered without any of the technical difficulties associated with Monte Carlo sampling. Furthermore, the approach can incorporate arbitrary level densities of the internal fragments. The disadvantage of such recursive techniques is that explicit *N*-body interactions (beyond mean field and Wigner-Seitz treatments) are ignored.

Before further discussion, one should review the validity of the physical assumptions in all statistical approaches. First, they should not be applied at densities higher than $\approx$ one-fourth of normal nuclear density. The approaches assume that the individual nuclei are well defined. As pointed out by Gross, fission of a spherical drop into two equal drops requires at least four times the volume of the original drop. At temperatures near T_c, where the density of the liquid phase falls, the range of treatable densities might be pushed even lower. Although fission is an extreme example, one can understand the importance played by geometry in fragment-fragment correlations by considering the fission example. The available volume for a large fragment clearly depends on the fragmentative state of the remainder of the system. The question of when the excluded-volume approximation is valid remains an open and intriguing question.

Secondly, one should keep in mind that nuclear collisions are dynamic processes. At excitation energies per nucleon much less than 5 MeV, fragment production occurs via evaporation, and the picture of a sudden disassociation where nucleons sample all states within a large volume is not reasonable. Even when sufficient excitation energy allows the nucleus to explode, individual nucleons and light clusters have had the chance to evaporate from the expanding surface while larger clusters have not had time to sample the same volume as the faster lighter fragments. Of course angular momentum can play an important role in fragment emission.

Finally, the incorporation of Coulomb is problematic in a statistical picture. In the MMMC model, where Coulomb is explicitly included, the larger fragments push to the outside of the boundary so as to minimize the Coulomb energy. Dynamics favor the opposite trend as large fragments require more time to move to the periphery. The Coulomb rearrangement energies may be many tens of MeV, which is much less than the overall excitation energy, but is much greater than the temperatures of interest. Simple Wigner-Seitz pictures, as presented here or in the SMM model, can make only gross estimates of the effect of the Coulomb force. However, it is not clear whether the more sophisticated Coulomb treatment of the MMMC model is more consistent with the true physical situation.

The immediate goals of this investigation are twofold. First, we wish to explore whether the recursive approaches can be extended to include microcanonical constraints and fragment-fragment interactions, and whether the techniques can be developed to make exact calculations of multiplicity distributions, which are not trivially derived from the partition function. Secondly, we wish to investigate the possibility that fragmentation observables are related to fundamental properties of the liquid-vapor phase transition, and to understand how such signals are affected by energy conservation, Coulomb effects and interfragment interactions. In this paper, the recursive approach is pursued for our studies. This choice is motivated by the rapid calculation times, the lack of Monte Carlo methods, and the ability to compare canonical and microcanonical calculations of identical systems.

III. MULTIPLICITY DISTRIBUTIONS AND THE CORRELATION COEFFICIENT

Multiplicity distributions are often described by two parameters, the mean and variance. In this section we discuss the correlation coefficient ξ which parametrizes the variance relative to the mean in such a way that it can be viewed as a correlation. A super- or sub-Poissonian multiplicity distribution is one whose variance exceeds or falls below its mean, respectively. The difference of the variance and the mean can also be written as a correlation. We demonstrate this by considering the emission into an arbitrarily large number of states *i*, each of which is infinitesimally probable. A state could be defined as a specific type of IMF emitted into an arbitrarily small bin in momentum space. The difference of the variance and the mean is

$$\begin{aligned}\sigma^2-\langle n\rangle &= \sum_{i,j}\ (\langle n_i-\langle n_i\rangle)(n_j-\langle n_j\rangle)-\sum_i\ \langle n_i\rangle \\ &= \sum_{i\neq j}\ (\langle n_i-\langle n_i\rangle)(n_j-\langle n_j\rangle) \\ &\quad +\sum_i\ (\langle n_i-\langle n_i\rangle)^2-\langle n_i\rangle. \qquad (1)\end{aligned}$$

If the bins are arbitrarily small, one may discard the terms in

the second sum proportional to $\langle n_i\rangle^2$, then use the fact that $n_i^2=n_i$ for $n_i=0$ or 1, to discard the remainder of the second term and obtain

$$\xi\equiv\frac{\sigma^2-\langle n\rangle}{\langle n\rangle^2}=\frac{\sum_{i\neq j}\langle(n_i-\langle n_i\rangle)(n_j-\langle n_j\rangle)\rangle}{\langle n\rangle^2}. \tag{2}$$

Here, ξ can be interpreted as a correlation coefficient. It is positive if the emission into two different bins is positively correlated. The only assumption going into this derivation is that the bins may be divided into arbitrarily small sizes.

The simplest examples of sub- and super-Poissonian multiplicity distributions are the binomial and negative-binomial distributions. The binomial distribution is defined in terms of two parameters p and N:

$$P_n=\frac{N!}{n!(N-n)!}p^n(1-p)^{N-n}, \tag{3}$$

where p is the probability of success in one of N tries. For the binomial distribution the mean and correlation coefficients become

$$\langle n\rangle_{\rm bin}=pN, \tag{4}$$

$$\xi_{\rm bin}=-1/N, \tag{5}$$

and stays negative. As with most correlations it is proportional to the inverse of the system size.

The negative-binomial distribution is also defined by two parameters p and N,

$$P_n=\frac{(N+n-1)!}{(N-1)!n!}\frac{p^n}{(1+p)^{N+n}}. \tag{6}$$

The correlation coefficient in this case is opposite to that of the binomial distribution:

$$\langle n\rangle_{\rm neg\ bin}=pN, \tag{7}$$

$$\xi_{\rm neg\ bin}=1/N. \tag{8}$$

Binomial and negative-binomial distributions result when one considers populating N quantum levels with fermions or bosons respectively with p representing the average population of each level.

Random emission from a large number of uncorrelated sources leads to a Poissonian distribution. The binomial distribution suggests that conservation of particle number would give a negative correlation coefficient of order $1/N$, where $N=A/a$ is the number of intermediate-mass fragments of characteristic size a that could fit into the system. For sufficiently small systems, this negative contribution from particle-number conservation dominates, with the extreme case being where a is more than half the system size meaning that no more than one IMF can be emitted. Other negative correlations are expected due to energy conservation. If IMF emission requires energy, e.g., escaping a Coulomb barrier, energy conservation is expected to reduce the probability of emitting a second IMF. We will see in the next sections that positive correlations can arise in canonical treatments both in the region of the phase transition and at low temperature due to surface effects.

Aside from the size of the correlations, it is also of interest to understand whether the entire multiplicity distribution, is well described by a two-parameter fit to a binomial or negative-binomial distribution. If the reduction of the results to two parameters is valid, comparison of different models and data is greatly simplified.

IV. RECURSION RELATIONS FOR CALCULATING FRAGMENTATION OBSERVABLES

A. The canonical ensemble

Chase and Mekjian have shown that canonical partition functions can be easily calculated in terms of the partition functions of single clusters. This allows the calculation of thermodynamic quantities for a system of fixed nucleon number without resorting to numerically intensive Monte Carlo procedures. If the partition function for a single cluster of size a_k is denoted by ω_k, the partition function for a system of size A may be written

$$\Omega_A\equiv\sum_{\langle\Sigma n_k a_k=A\rangle}\prod_k\frac{\omega_k^{n_k}}{n_k!}=\sum_k\omega_k\frac{a_k}{A}\Omega_{A-a_k}. \tag{9}$$

Thus, Ω_A is expressed recursively in terms of ω_k and $\Omega_{A'}$ for $A'<A$. Proof of this relation is given in the Appendix. The only shortcoming of this approach is that explicit (not mean field) interactions between fragments are ignored.

Moments of the multiplicity distribution may be expressed in terms of the partition functions. The moments can then be used to derive the correlation coefficient, ξ_a defined in Eq. (2) or the multiplicity distribution as discussed below. The first moment is the mean which is defined as

$$\langle n_k\rangle=\omega_k\frac{\Omega_{A-a_k}}{\Omega_A}. \tag{10}$$

Rather than considering moments $\langle n_b^m\rangle$ it is more convenient to consider factorial moments $F_{b,A,m}$ defined as

$$F_{b,A,m}\equiv\langle n_b(n_b-1)\cdots(n_b-m+1)\rangle. \tag{11}$$

Calculation of the factorial moments for n_b defined in Eq. (11) is simple if b refers to single species k:

$$F_{k,A,m}=\omega_k^m\frac{\Omega_{A-ma_k}}{\Omega_A}. \tag{12}$$

However, if b refers to a set of species, $n_b=\Sigma_{k\in b}n_k$, where the various species that comprise b have different masses, Eq. (12) is no longer valid. One must then generate the factorial moments using the recursion relation

$$F_{b,A,m}=\sum_{k\in b}\omega_k F_{b,A-a_k,m-1}\frac{\Omega_{A-a_k}}{\Omega_A}, \tag{13}$$

which is true in general. The proofs of Eqs. (12) and (13) are given in the second section of the Appendix.

As shown in the third subsection of the Appendix, factorial moments are sufficient for calculating the entire multiplicity distribution via the relation

$$P_{b,A,n}=\sum_{m\geqslant n} F_{b,A,m}\frac{1}{(m-n)!n!}(-1)^{m-n}, \tag{14}$$

where $P_{b,A,n}$ gives the probability of viewing n fragments of type b in a system of size A. More directly, one may also generate the multiplicity distribution, without knowing the factorial moments, through the recursion relation

$$P_{b,A,n}=\frac{1}{n}\sum_{k\in b}\omega_k P_{b,A-a_k,n-1}\frac{\Omega_{A-a_k}}{\Omega_A}. \tag{15}$$

Proof of Eq. (15) is presented in the Appendix. This direct method of producing the multiplicity distribution has proven more numerically stable than generating the distribution from the factorial moments. This improvement can be traced to the alternating signs in Eq. (14).

Summarizing the technique, one starts by calculating partition functions for individual fragments ω_k. One may then generate partition functions, Ω_A, by using the recursion relation, Eq. (9). The recursion relation for factorial moments, Eq. (13), then allows one to generate the factorial moments, which in turn allow the determination of the entire multiplicity distribution using Eq. (14). Alternatively, one may calculate the multiplicity distributions directly using Eq. (15). The obtained multiplicity distributions are exact. Although the sums used in the recursion relation are performed numerically, they require only a fraction of a second of computer time.

B. Microcanonical calculations

A microcanonical approach, which considers configurations only at a specific energy, would be more realistic for application to nuclear phenomenology since nuclear collisions do not take place with contact to a heat bath. The importance of performing microcanonical calculations is emphasized by the existence of the first order phase transition, which collapses a wide range of energy densities to a narrow range of temperatures. In this section we present expressions for calculating fragmentation observables within a microcanonical context.

It is straightforward to obtain the needed microcanonical quantities from the expressions for partition functions by Fourier transforming corresponding canonical objects over a range of complex $\beta\equiv 1/T$. For instance, the level density, $\rho(E)$, may be obtained from the partition functions through

$$\rho(E)=\mathrm{Tr}_{\alpha}\delta(E-E_{\alpha})=\frac{1}{2\pi}\int d\beta\Omega_A(i\beta)e^{i\beta E}. \tag{16}$$

One may calculate recursion relations for the factorial moments and for the multiplicity distributions at fixed energy. First we consider $f_{b,A,m}(i\beta)$ and $p_{b,A,n}(i\beta)$, which are the canonical quantities without the normalization brought on by dividing by Ω. As described in the Appendix, they may be found via recursion relations

$$f_{b,A,m}(\beta)\equiv\Omega_A(\beta)F_{b,A,m}(\beta)=\sum_{k\in b}\omega_k f_{b,A-a_k,m-1}(\beta), \tag{17}$$

$$p_{b,A,n}(\beta)\equiv\Omega_A(\beta)p_{b,A,n}(\beta)=\frac{1}{n}\sum_{k\in b}\omega_k p_{b,A-a_k,n-1}(\beta). \tag{18}$$

The factorial moments and multiplicity distributions at fixed energy E may then be expressed as

$$F_{b,A,m}(E)=\frac{\int d\beta f_{b,A,m}(i\beta)e^{i\beta E}}{2\pi\rho(E)}, \tag{19}$$

$$P_{b,A,n}(E)=\frac{\int d\beta p_{b,A,n}(i\beta)e^{i\beta E}}{2\pi\rho(E)}.$$

However, the integrations over β needed to obtain the relevant microcanonical quantities do make the calculations significantly more numerically intensive. It is not clear to what degree the stationary-phase approximation [22] might allow one to avert the numerically costly integration, especially given the first order phase transition which causes discontinuities as a function of β.

If one is interested in the microcanonical distribution, for a range of energies in the neighborhood of E, rather than for an exact value of E, one may replace the delta function in Eq. (16) by a Gaussian

$$\delta(E-E_{\alpha})\rightarrow\frac{1}{\sqrt{2\pi\eta^2}}\exp-\frac{(E-E_{\alpha})^2}{2\eta^2}, \tag{20}$$

where η defines the width of the neighborhood. One may incorporate the broadening of the δ function by modifying the phase factors used in the Fourier transforms

$$e^{i\beta E}\rightarrow e^{i\beta E}\exp-\frac{1}{2}\eta^2\beta^2. \tag{21}$$

Numerical implementation of the Fourier transform simplifies for broader widths η, as it effectively narrows the required integration range for β.

An alternative way to approach the constraint of energy conservation is to discretize the energy and measure it with integral values. One can then treat energy in the same manner with which one would treat other conserved charges. For instance, energy might by measured in steps of 0.5 MeV, with an integer Q measuring the energy. If ω_{i,q_i} counts the number of states available to a particle of type i with energy q_i and mass a_i, the number of states of the system of mass A with net energy Q becomes

$$N(A,Q)=\sum_{\langle \Sigma n_i a_i=A,\Sigma n_i q_i=Q\rangle}\Pi\frac{\omega_{i,q_i}^{n_i}}{n_i!}. \tag{22}$$

One may then derive the recursion relation in a manner similar to the derivation of the recursion relation for the partition function shown in Sec. VII A. Since there are two conserved ''charges,'' two recursion relations may be derived,

$$N(A,Q)=\sum_{i,q_i}\frac{a_i}{A}\omega_{i,q_i}N(A-a_i,Q-q_i), \tag{23}$$

$$=\sum_{i,q_i}\frac{q_i}{Q}\omega_{i,q_i}N(A-a_i,Q-q_i). \tag{24}$$

In a manner similar to the derivations in Secs. VII B and VII D one may derive recursion relations for the factorial moments and multiplicity distributions

$$F_{b,A,Q,m}=\sum_{k\in b,q_k}\omega_{k,q_k}F_{b,A-a_k,Q-q_k,m-1}\frac{N(A-a_k,Q-q_k)}{N(A,Q)}, \tag{25}$$

$$P_{b,A,Q,n}=\sum_{k\in b,q_k}\omega_{k,q_k}\frac{1}{n}P_{b,A-a_k,Q-q_k,n-1}\times\frac{N(A-a_k,Q-q_k)}{N(A,Q)}. \tag{26}$$

There are two practical differences between these expressions and the corresponding canonical expressions. First, an extra index has been added that denotes the energy of the system. In practice this leads to a longer calculation by a factor of the number of energy steps squared. Thus if one wishes to perform a microcanonical calculation with an excitation energy of one GeV, using energy steps of 1.0 MeV, the required computer time would be expected to increase by 10^6 as compared to a canonical calculation at a single temperature.

Knowing the number of ways to arrange a system of size A into energy Q allows one to determine the temperature T:

$$\frac{1}{T}=\frac{\partial \ln N_{A,Q}}{\partial Q}. \tag{27}$$

Mass distributions are straightforward to generate from $N_{A,Q}$:

$$\langle n_k\rangle=\frac{\Sigma_{q_k}\omega_{k,q_k}N_{A-a_k,Q-q_k}}{N_{A,Q}}. \tag{28}$$

C. Generating random events and including hard-sphere interactions

Although the recursion relations of the previous sections allow the exact calculation of nearly any observable, one may wish to randomly generate individual events consistent with the partition functions. This may be useful for filtering through experimental acceptances or for calculating the effects of Coulomb trajectories on outgoing particles. Later in this paper, random events will be utilized to calculate the effects of hard-sphere fragment-fragment interactions.

Events are generated fragment-by-fragment. The first fragment is generated from a system of size A according to the weight

$$w_k=\frac{a_k}{A}\omega_k\frac{\Omega_{A-a_k}}{\Omega_A}. \tag{29}$$

After the first fragment is generated, a second fragment may be generated using $A-a_k$ in place of A for the weight. Similarly, one may generate events in a microcanonical ensemble using the weights

$$w_{k,q_k}=\frac{a_k}{A}\omega_{k,q_k}\frac{N_{A-a_k,Q-q_k}}{N_{A,Q}}. \tag{30}$$

Hard-sphere interactions between fragments may be included by generating a sample of events and discarding any event where two fragments overlap. The total number of events is then the original number, $N_{A,Q}$ in the microcanonical case, multiplied by the fraction of events that pass the filter. Given that this procedure entails randomly placing the fragments in the volume and testing all pairwise overlaps, it can certainly become numerically prohibitive when the fragment multiplicity becomes large. At some point Metropolis techniques such as those incorporated into the MMMC model become necessary.

V. RESULTS

A. A liquid-drop example in the canonical ensemble

For our purposes, we consider the partition function for individual fragments of mass k as

$$\omega_k=V\left\{\frac{a_k MT}{2\pi}\right\}^{3/2}e^{-F_{k,\mathrm{int}}/T}, \tag{31}$$

$$F_{k,\mathrm{int}}=f_b a_k+f_s a_k^{2/3}+f_c\frac{1}{4}a_k^{5/3}, \tag{32}$$

where the volume of the system is V, the mass of a single nucleon is M, and the fragment's internal free energy $F_{k,\mathrm{int}}$ is split into a bulk term and a surface term. One sees that the bulk term is irrelevant in determining fragmentation observables since it factors out of the partition function. Thus, aside from the system size A, all fragmentation observables are determined by three parameters, the ratio of the surface term to the temperature f_s/T, the specific entropy, $s\equiv(V/A)(MT)^{3/2}$, and Coulomb term, f_c. This implies that many details of a system's microscopic makeup, e.g., Fermi vs Bose nature of the internal excitation, are irrelevant in determining the statistics of fragmentation. If the surface term is negligible fragmentation is determined purely by the specific entropy.

For the surface and Coulomb terms, we use the parameters of the nuclear liquid-drop model

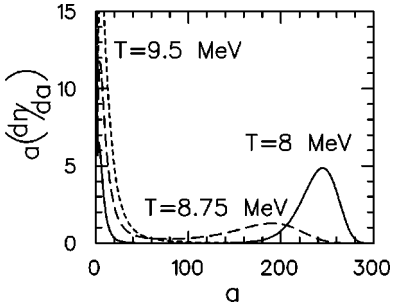

FIG. 1. Mass distributions are displayed (scaled by a) at three temperatures for an $A=300$ system. At the high temperature, 9.5 MeV (short dashes), the distribution is dominated by small fragments, while below the fragmentation threshold, at 8 MeV (solid line), most nucleons reside in one fragment. At the intermediate temperature, 8.75 MeV (dashed line), the mass seems equally divided between the large cluster and small clusters. The transition occurs over a remarkably narrow range of temperatures.

$$f_s = 17.2 \ \text{MeV}, \tag{33}$$

$$f_c = 0.70\left(1-\left(\frac{\rho}{\rho_0}\right)^{1/3}\right)\text{MeV}, \tag{34}$$

where the form of the Coulomb term was taken to account for the screening of the Coulomb repulsion by the nuclear medium in a Wigner-Seitz-like parametrization [13] with ρ_0 referring to nuclear saturation density of $\rho_0^{-1}=(4\pi/3)r_s^3$, where $r_s=1.2$ fm.

All the calculations presented in this paper assumed a density of one-sixth of nuclear matter density. The behavior at different densities is not qualitatively different, with the exception of the relative importance of the Coulomb term. The fragmentation transition described below occurs when $s=(1/\rho)(mT)^{3/2}$ is of order unity. Therefore a change of density affects the temperature where fragmentation sets in. An excluded volume could easily be incorporated into the problem by replacing V with V_{eff}. This is equivalent to changing the density, and does not qualitatively affect the results. The surface energy is chosen to be a constant, $f_s=17.2$ MeV. One could imagine scaling f_s as a function of density or temperature, although one might object to incorporating a temperature dependence that is not of the nature $e^{E/T}$. The choice of f_s does affect the transition temperature and its width. Larger choices of f_s lead to sharper transitions. For these calculations we assume a density of one-sixth normal nuclear density, but choose three-fourths of the volume to account for exclude volume. Thus the volume is effectively 4.5 times the volume of a nucleus of size A. However, the factor of one-sixth does come into play when considering the Coulomb corrections.

In Fig. 1, the mass distribution dN/da is shown for three temperatures $T=8.0$, 8.75, and 9.5 MeV. The overall size of the system was chosen to be 300 and Coulomb effects were neglected in these calculations. The mass distribution has been multiplied by a to emphasize how the nucleons are partitioned into the various sized drops. The mass distribution changes dramatically within a small temperature range.

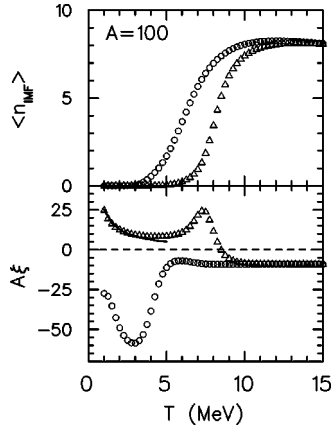

FIG. 2. The average multiplicity of IMFs, those fragments with masses from 5 to 40, is shown in the upper panel as a function of temperature for an $A=100$ system. Including Coulomb (circles) lowers the threshold temperature for fragmentation compared to when Coulomb is ignored (triangles). Correlation coefficients are displayed in the lower panel. The approximations described in the text, which are represented by lines, describe the behavior at low excitation. A positive correlation at the fragmentation threshold arises from two classes of events with different exciation energies, those with and without a large cluster, which both contribute at the fragmentation threshold.

The average multiplicity of intermediate-mass fragments ($5<a\leqslant 40$), denoted as IMFs, are shown in the upper panel of Fig. 2 for a system of size $A=100$. Results are plotted against the temperature, both for the case where the Coulomb term is included as well as for the case where it is neglected. The inclusion of Coulomb pushes fragmentation down towards lower temperatures. The trend would strengthen if we were to consider larger systems. When the excitation energy exceeds the fragmentation threshold, average IMF multiplicities quickly climb to over a half-dozen per event. Correlation coefficients are shown in the lower panel of Fig. 2. Coefficients are shown both for the case where Coulomb is included and for the case where Coulomb is neglected.

When Coulomb is neglected super-Poissonian behavior ensues at lower excitations as evidenced by the positive values of ξ. At low temperatures, this behavior may be understood by considering the surface penalty for emitting a single fragment of mass a,

$$\Gamma(A\rightarrow A-a)\propto\exp\left\{-a\ \frac{d}{dA}(F_{\text{surf}}/T)\right\}. \tag{35}$$

If a second IMF is emitted, it feels the same penalty, except for the fact that dF/dA is evaluated at a smaller overall size $A-a$. The correlation becomes

$$\xi_{\text{surf}}\approx\frac{\Gamma(A\rightarrow A-a)\Gamma(A-a\rightarrow A-2a)}{\Gamma(A\rightarrow A-a)^2}-1 \tag{36}$$

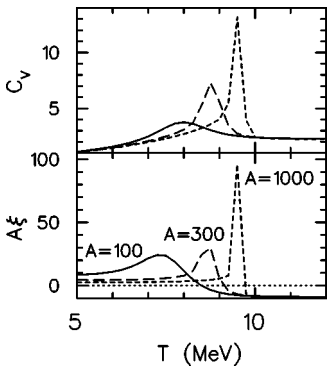

FIG. 3. The evolution of the correlation coefficient is shown for a small range of temperatures for increasingly large system sizes in the lower panel. For large systems the peak narrows into a singularity, a signal of discontinuous behavior. Nearly identical behavior is seen in the specific heat per particle which is displayed in the upper panel. Coulomb has been neglected in these calculations.

$$\approx \frac{a^2}{T}\frac{d^2F_{\rm surf}}{dA^2}$$

$$= \frac{2a^2 f_s}{9T}A^{-4/3}.$$

The dashed line represents the surface contribution to ξ and closely follows the statistical calculation at lower temperatures. The average size of an IMF was used for a.

The inclusion of Coulomb reduced ξ to negative values as seen in Fig. 2. The Coulomb contribution to ξ may be approximated in a similar fashion as the surface contribution

$$\xi_{\rm Coul} \approx -\frac{5a^2 f_c}{9T}A^{-1/3}. \tag{37}$$

The simple estimate of ξ works well at low temperature when Coulomb is neglected, as most of the particles reside in a single fragment. The approximations for ξ are poor for large systems when Coulomb is included. This arises because a large system does not wish to form a single drop when Coulomb is included.

At high temperatures the sub-Poissonian behavior may be roughly understood as arising from particle conservation. As seen in Sec. III when considering binomial distributions, one expects a negative correlation of order $1/N$, where N is the maximum number of IMFs that fit into the system.

The super-Poissonian (or nearly super-Poissonian when Coulomb is included) behavior at the fragmentation threshold is especially interesting. Perhaps this may be understood by stating that the partition function is sampling two competing configurations, one with one large fragment surrounded by gas and a second one where numerous IMFs are present. These configurations have significantly different energies. At the fragmentation threshold, where the system is undergoing a transition, both configurations occur leading to a broadened multiplicity distribution. Figure 3 displays ξ, again scaled by A, as a function of temperatures between 5 and 12 MeV, for three sizes $A=100$, $A=300$, and $A=1000$. Coulomb is ignored in these calculations. As the system size increases a singularity in ξ develops at the boiling temperature. This is related to a discontinuity in the energy vs temperature at constant volume [20], which is characteristic of this model but not necessarily characteristic of a typical liquid-gas transition. In a liquid-gas transition C_p becomes singular but not C_V. Since the peak in ξ vs T is linked to the discontinuity in the energy density at the same temperature, the peak might disappear in a microcanonical treatment.

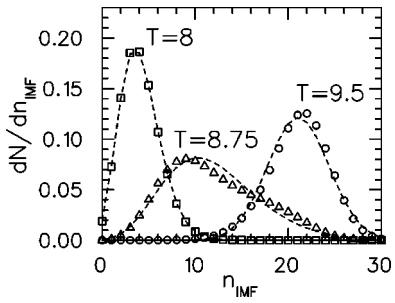

FIG. 4. Multiplicity distributions are shown at three temperatures for the $A=300$ system. Below the fragmentation threshold at a temperature of 8 MeV (squares), the distribution is peaked at a low multiplicity and is well described by a negative-binomial distribution shown as a dashed line. At a high temperature of 9.5 MeV (circles), the distribution is sub-Poissonian and well described by the binomial distribution (dashed line). At 8.75 MeV (triangles), the multiplicity distribution is strongly super-Poissonian and is not well described by a negative binomial.

The multiplicity distributions for the $A=300$ system with Coulomb ignored are shown in Fig. 4 for three temperatures. They are compared to negative-binomial and binomial distributions, respectively, where the two parameters are chosen to fit the mean and variance of the distributions. At the intermediate temperature, the distribution's shape is less well described by a negative-binomial fit. This emphasizes that two classes of events, corresponding to the two phases, contribute at this temperature.

B. Microcanonical results

Analogous calculations to those of the previous subsection were performed for the microcanonical case. In order to perform the microcanonical calculations, energy was discretized in units of 2.0 MeV. The internal nuclear levels were modeled by assuming each nucleus had uniformly spaced single-particle levels, with the single-particle level density for a nucleus of mass a_k being

$$g_k = (a_k - 1)\frac{\pi^2}{6\epsilon_0}, \tag{38}$$

with ϵ_0 being equal to 12 MeV. The levels of the nuclear composite were found by accounting for all ways to arrange individual fermions in the uniformly spaced levels at a given total energy. This was accomplished through a simple counting algorithm [23,24]. Explicitly counting the levels gives the same answer as Eq. (39) at high excitation:

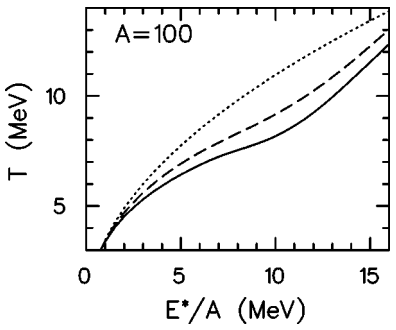

FIG. 5. The temperature is plotted against the energy density for the microcanonical (solid line) calculation, canonical (dashed line) calculation, and the low-temperature Fermi gas expansion (dotted line). The calculations were performed for a system of size $A=100$ without Coulomb. The transitions of the caloric curve are somewhat sharper in the microcanonical case.

$$\rho_{\text{internal}}(E^*) = \frac{1}{\sqrt{48}E^*} \exp\sqrt{2a_k E^*/\epsilon_0}. \tag{39}$$

For the monomers, $a_k=1$, a degeneracy of four was chosen.

The density of states of single fragments was found through convoluting the kinetic and internal energies:

$$\rho_k(E) = \frac{Vm_k}{2\pi^2\hbar^3} \int dE_{\text{kin}} \sqrt{2m_k E_{\text{kin}}}\, \rho_{k,\text{int}}(E - E_{\text{kin}} - E_{\text{LD}}), \tag{40}$$

where E_{LD} is the liquid-drop energy of the nucleus of type k which includes a bulk term, a surface term and a Coulomb term. Once ρ is calculated, the number of quantum states available to a single cluster within a discretized energy window is determined. These form the basis for the recursive algorithms used to generate the number of states of the many-particle system with a given energy.

Temperatures were calculated by taking the logarithmic derivative of the system's level density with respect to the energy, and are shown in Fig. 5. The result is compared to the canonical equivalent, where the energy is determined by taking the derivative of the canonical partition function with respect to T, with the canonical partition functions being generated with the same set of nuclear states. The canonical and microcanonical results are similar, but the microcanonical curve is characterized by a somewhat sharper transition. Finer energy discretizations of 1.0 MeV were also tried and gave identical results for the caloric curve.

Mass distributions, multiplied by the size of the fragment a, are shown in Fig. 6 at three excitations. As expected, at low excitation most of the mass exists in the form of large clusters while at high excitation most of the mass resides within small fragments.

Multiplicity distributions were generated with the use of Eq. (26) and are displayed in Fig. 7 for three excitations. They are well fit by binomial distributions where the binomial parameters p and N were determined by fitting the mean and variance of the distributions. Unlike the canonical calculations, the microcanonical calculations always returned sub-Poissonian multiplicity distributions.

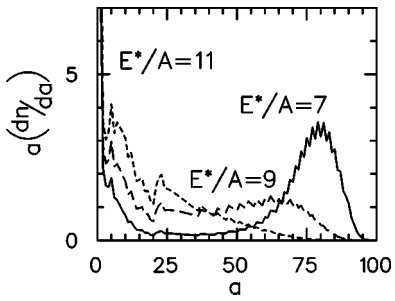

FIG. 6. Mass distributions generated from microcanonical calculations are shown for a system of size $A=100$ without Coulomb for three different excitations, $E/A=7$, 9, and 11 MeV/nucleon. The jagged lines result from the discretizaton of the energy.

The mean and correlation coefficient were generated from the IMF multiplicity distributions and are presented in Fig. 8. Results are shown both for the case where Coulomb is included and where it is neglected. The inclusion of Coulomb lowers the threshold for fragmentation as expected. The correlation coefficient is of a different character when calculated for a microcanonical calculation. When Coulomb is neglected, the correlation coefficient is positive for canonical calculations as was shown in the previous subsection. This was related to the sharp change in the energy density as a function of temperature, which allowed the canonical ensemble at a fixed temperature to include substantive weightings from a wide range of energies, thus sampling both liquidlike and gaslike configurations simultaneously. The correlation coefficient for the microcanonical case also exhibits a maximum at an excitation in the center of the liquid-gas transition region. However, this maximum does not become increasingly sharp with increased system size and can therefore not be considered as a signal of a phase transition. Also, the contribution from surface energy which yields a positive contribution in the canonical example has the opposite effect in the microcanonical example. For the microcanonical case, the emission of a first fragment uses valuable energy needed for the subsequent emission of a second frag-

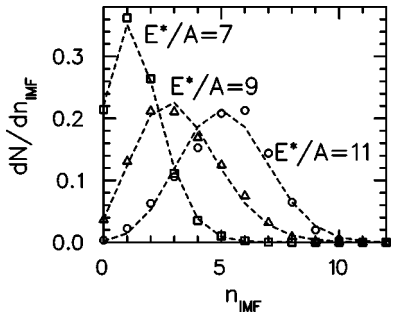

FIG. 7. Multiplicity distributions of IMFs as generated from a microcanonical ensemble are displayed for three excitations, $E/A=7$ MeV (squares), 9 MeV/nucleon (triangles), and 11 MeV/nucleon (circles). Calculations assumed a size $A=100$ and ignored Coulomb effects. The distributions are fairly well described by binomial distributions (dashed lines).

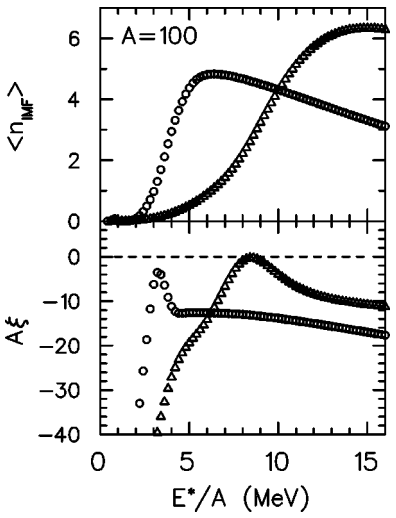

FIG. 8. The average number of IMFs and the correlation coefficient as generated from a microcanonical calculation for a mass $A=100$ system are shown with (cirlces) and without (triangles) Coulomb. The inclusion of Coulomb reduces the amount of energy needed for fragmentation. Whereas canonical calculations yield a sharp peak in the correlation coefficient, microcanonical calculations reveal a broad maximum. Even when Coulomb is neglected, the IMF multiplicity distributions remain sub-Poissonian at all excitations.

ment. A noticeable peak resulted for the microcanonical calculation of ξ with Coulomb. However, we note that this peak was rather sensitive to details of the breakup density and might well be related to fissionlike geometries.

Even though the sharp peak disappears in the microcanonical case, the behavior of the correlation coefficient in the critical region is interesting. The coefficient approaches zero, and if fit to a binomial distribution would suggest that the limiting number of fragments $1/\xi$, would surpass the cutoff due to particle-number conservation. Furthermore, the behavior of ξ with energy is qualitatively different from what is predicted from percolation calculations [25].

In nuclear experiments one can directly adjust the excitation energy, and since there is no external heat bath, microcanonical descriptions are more appropriate. However, one could justify a canonical language by binning events according to the kinetic energy of the fragments while taking samples from events with a wide variety of excitations. One could then treat the kinetic component of the energy as a heat bath for the fragmentative degrees of freedom. This is rather artificial and the finite size of the kinetic energy would not truly represent a heat bath, but such an analysis might well result in discontinuous observables plotted against an effective temperature.

Finally, we remark on the computational time required to perform microcanonical calculations using the recursive techniques listed above. While canonical calculations for one temperature can be performed in a fraction of a second on any modern workstation, microcanonical calculations require significantly more computational effort. Using a 500 MHz Pentium CPU, microcanonical calculations of the caloric curve and mass distributions required approximately one minute. Calculating the multiplicity distribution required approximately 10 min. These calculations were performed for a system of mass 100, without inclusion of isospin. We estimate that doubling the system size and including isospin could increase the computational requirements by two to three orders of magnitude. Calculations of the multiplicity distribution might then require as much as a few days of CPU time, while calculations of the partition functions, mass distributions or lower moments would require a few hours. We emphasize that the recursive nature of these calculations implies that the quantities are always calculated at every excitation at once, thus one does not need to repeat the calculation for every energy. Of course, if the volume varies with excitation [26], one would still need to run the calculation several times. It should be noted that since calculations require a time proportional to the square of the maximum excitation energy, calculations proceed quite rapidly if range of excitation energies remains less than 8 MeV per nucleon.

C. Repulsive spheres and excluded volume

The calculations of the previous two sections assumed the available volume for all fragments was 4.5 times the volume of A nucleons:

$$V_{\mathrm{eff}}=\frac{3}{4}6Ar_s^3, \tag{41}$$

where r_s was chosen to be 1.2 fm. Choosing a density of $\rho_0/6$ is somewhat arbitrary, but is consistent with the density of the MMMC model. Excluding one-fourth of the volume was motivated by the empirical observation that randomly generated events survived without overlap with a factor $(3/4)^{\overline{N}-1}$, where $\overline{N}$ is the average multiplicity.

Thus, the procedure for including hard-sphere repulsion is (1) calculate the microcanonical partition functions, $N_{A,E*}$, assuming a breakup density of one-sixth normal nuclear density, (2) generate events according to the procedure described in Eq. (30), (3) discard any events where the separation between any two fragments i and j is less than $r_s(a_i^{1/3}+r_j^{1/3})-r_s$, (4) modify the partition function according to the fraction f of events that survive the overlap criteria $N_{A,E*}\rightarrow fN_{A,E*}$, (5) use the generated events to find multiplicity distributions and moments. As mentioned above, the fraction of events that survived the overlap criteria was approximately $(3/4)^{\overline{N}-1}$, which motivated our choice of excluded volume in the previous subsections.

Figure 9 displays the caloric curve for the case where hard-sphere repulsion is included, and is compared to the results where the excluded-volume approximation was applied. The two results are remarkably similar. Unlike the results presented here, the temperature calculated from the MMMC model fell with temperature [27] in the transition region. The temperature rose monotonically with excitation energy in all the calculations performed in this study. The monotonic behavior is a requirement in a canonical model, but is not so clear in a microcanonical treatment. This qualitative difference in behavior might be due to different treatment of Coulomb in the two pictures. Since the MMMC

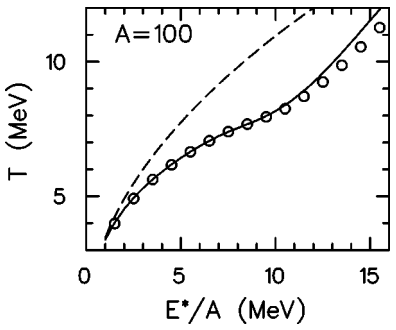

FIG. 9. The caloric curve is shown both for the case where hard-sphere interactions are accounted for by randomly generating events and discarding those with spatial overlaps (circles) and for the case where the excluded-volume approximation is implemented (solid line). The dashed line represents the Fermi-gas approximation. The excluded volume approximation appears quite successful for describing the caloric curve at one-sixth saturation density.

method is based on Metropolis sampling, explicit fragment-fragment interactions can be incorporated including the long-range Coulomb force. Running the MMMC model without Coulomb interactions might clarify the issue.

The IMF multiplicity and correlation coefficients are displayed in Fig. 10. Again the results are very similar to the calculations using the excluded-volume approximation, although one expects the excluded-volume approximation to fail at higher densities. These calculations were performed with 160 thousand events, and the statistical error bars are smaller than the size of the symbols in the plot. One should emphasize that other forms of fragment-fragment interactions might affect the correlation coefficient more noticably. Hard-sphere interactions are the simplest to incorporate into the partition functions as those events that are not discarded do not have their energy affected by the interaction.

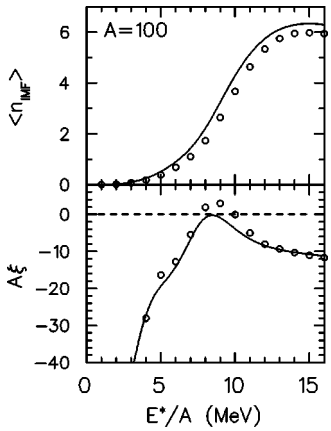

FIG. 10. The average number of IMFs and the correlation coefficient as generated from a microcanonical calculation for a mass $A=100$ system are shown for the calculations using the excluded volume approximation (solid line) and for the case where fragment-fragment overlaps are excluded by sampling randomly generated events. The geometrical constraints of hard-sphere potentials seem to be well accounted for with the excluded volume approximation for these calculations which are done at one-sixth saturation density.

The process of generating random events from the partition function is extremely quick, and might replace the process of exact generation of the multiplicity distributions which was rather numerically intensive. However, invoking the fragment-overlap criteria greatly slowed the process of generating events at high temperatures when multiplicities were high. For multiplicities of 40, only one in 100 000 events might survive the overlap criteria.

VI. CONCLUSIONS

This paper had two principal aims. First, we wished to determine the limits to which Mekjian's recursive methods could be extended to calculate fragmentation observables. To that end, several new recursion relations were discovered that make possible the exact calculation of the entire multiplicity distribution as well as the associated factorial moments. Expressions were also derived that allow the generation of random events that are statistically consistent with the partition functions. By discarding events where fragments spatially overlapped with one another, it becomes possible to account for hard-sphere fragment-fragment interactions.

The recursive techniques were extremely quick when applied to the canonical case. However, significant computational effort would be required for microcanonical calculations should isospin conservation be added to the description. Calculations of the partition functions might then require many hours to cover the entire excitation-energy range of interest, and might require days if one wishes exact calculations of the multiplicity distributions. The generation of random events from the partition functions was also extremely quick, unless hard-sphere interactions were included, and could be used to bypass the potentially lengthy calculations of the multiplicity distributions. Even though calculations have the potential to be somewhat lengthy, the method has an appeal in that all configurations, including all divisions of excitation energy and particle number, were accounted for, thus bypassing some of the uncertainties inherent to Monte Carlo sampling.

Our second goal was to study whether fragmentation observables, especially those related to fluctuations of the IMF multiplicity distributions, carried a signal regarding the liquid-vapor phase transition. The correlation coefficient ξ was defined to describe the width of the IMF multiplicity distribution relative to it's mean in such a way that it is positive or negative for super- or sub-Poissonian distributions. The correlation coefficient developed a singularity at the critical point when plotted against the temperature in canonical calculations; whereas in microcanonical calculations ξ reached a gentle maximum for excitation energies in the fragmentation region. Even though the singular behavior of ξ was muted in a microcanonical treatment, the behavior of ξ as a function of the excitation energy was unique to the process of statistical fragmentation.

The sensitivity of the calculations to hard-sphere interactions and Coulomb interactions was also investigated. Hard-sphere interactions were fully implemented, but were found to be well accounted for by excluded-volume approximations at one sixth saturation density. One expects the excluded-volume approximation to fail at higher density, not only be-

cause of the complex geometrical constraints of fitting hard spheres together, but because the physical picture of well-defined fragments becomes unreasonable at some point. Coulomb interactions were found to lower the fragmentation threshold as expected and to also lower the IMF correlation coefficients. However, we emphasize that the role of Coulomb might be poorly accounted for in this approach where only a Wigner-Seitz approximation was implemented. Comparison of equivalent calculations with the MMMC approach, which fully accounts for Coulomb, would be welcomed. However, it should be kept in mind that at equilibrium large fragments move to the periphery of the system which is opposite to the reality of the experimental situation where the short time of the explosion favors the expansion of lighter fragments. Such problems are inherent to statistical models incorporating the long-range Coulomb force. Long-range forces imply long-range correlations which require long times to develop.

The recursive techniques described here can be made more realistic in two ways. First, the sum over intrinsic states, which here was performed in a liquid-drop context, can be replaced by a sum over realistic nuclear states without a significant cost in the time of the calculation. Secondly, isospin conservation may be included. It is straightforward to extend the recursion relations to two conserved charges [28] without significantly increasing the complexity of the approach, although the calculational times would likely increase from minutes to hours should both neutron and proton conservation be enforced in a microcanonical calculation.

Despite previous efforts such as the MMMC and SMM models as well as the efforts described in this work, several qualitative questions remain regarding statistical multifragmentation. Most importantly, the MMMC calculations showing a nonmonotonic dependence of the temperature with respect to excitation energy have not been observed from other calculations where the volume is kept fixed. The role of long-range Coulomb forces might explain this behavior, or it might arise from some other more mundane aspect of the modeling such as the choice of how to parametrize the level densities of individual nuclei. Understanding how the predictions of the models are affected by various assumptions and parameters is a prerequisite to making insightful comparisons with experimental data.

ACKNOWLEDGMENTS

This work was supported by the National Science Foundation, Grant No. PHY-96-05207.

APPENDIX: DERIVATION OF RECURSIONS RELATIONS USED IN CANONICAL ENSEMBLES

1. Recursion relation for the partition function

The recursion relation described here was first presented by Lee and Mekjian [29], and was first applied in a liquid-drop context by Chase and Mekjian [19]. The general relation for the partition function of noninteracting species is

$$\Omega_A = \sum_{\langle \Sigma n_k a_k = A \rangle} \prod_k \frac{\omega_k^{n_k}}{n_k!}, \tag{A1}$$

where ω_k is the partition function for a single particle of the species k which has size a_k. For each term in the sum, one can factor a term ω_k out of the partition function. By using the fact that $\Sigma n_k a_k / A = 1$, one may rewrite the partition function

$$\Omega_A = \sum_k \sum_{\langle \Sigma n_i a_i = A \rangle} \frac{n_k a_k}{A} \frac{\omega_k^{n_k}}{n_k!} \prod_{i \neq k} \frac{\omega_i^{n_i}}{n_i!} \tag{A2}$$

$$= \sum_k \omega_k \frac{a_k}{A} \sum_{\langle \Sigma n_i a_i = A - a_k \rangle} \prod_i \frac{\omega_i^{n_i}}{n_i!}. \tag{A3}$$

From combining this expression with Eq. (A1), one can extract the recursion relation

$$\Omega_A = \sum_k \omega_k \frac{a_k}{A} \Omega_{A - a_k}. \tag{A4}$$

2. The recursion relation for factorial moments

Factorial moments allow convenient calculation of the multiplicity distribution as seen in the subsequent subsection. Given the partition function Ω_A, the moments $F_{k,A,m}$ are trivial to calculate for an individual species k:

$$\begin{aligned} F_{k,A,m} &\equiv \langle n_k (n_k - 1)(n_k - 2) \cdots (n_k - m + 1) \rangle \\ &= \frac{1}{\Omega_A} \sum_{\langle \Sigma n_i a_i = A \rangle} n_k (n_k - 1) \cdots (n_k - m + 1) \prod_i \frac{\omega_i^{n_i}}{n_i!} \\ &= \omega_k^n \frac{\Omega_{A - m a_k}}{\Omega_A}. \end{aligned} \tag{A5}$$

However, they are more difficult to obtain when they are defined in terms of n_b comprised of several species with different masses

$$n_b = \sum_{k \in b} n_k. \tag{A6}$$

However, in this case one may proceed with the help of a recursion relation for the factorial moments. To derive the recursion relation, we consider the function f:

$$f_{A,m}(b) \equiv \sum_{\langle \Sigma n_k = A \rangle} \prod_k \frac{\omega_k^{n_k}}{n!} n_b (n_b - 1) \cdots (n_b - m + 1), \tag{A7}$$

$$F_{b,A,n} = \frac{f_{A,n}(b)}{\Omega_A}. \tag{A8}$$

For the first term $n_b = \Sigma_{k \in b} n_k$ in the sequence of m terms $n_b (n_b - 1) \cdots (n_b - m + 1)$, each power of n_k may be used to

cancel n_k in the factorial. By then factoring ω_k outside the sum over configurations, one may rewrite f as

$$f_{A,m}(b)=\sum_{k\in b}\omega_k \sum_{\langle \Sigma n_{k'}=A-a_{k'}\rangle}\prod_{k'}\frac{\omega_{k'}^{n_{k'}}}{n_{k'}!}n_b'(n_b'-1)\times(n_b'-2)\cdots(n_b'-m), \tag{A9}$$

where n_b' represents the number of b-type fragments in the set k', which differs from the previous set by the reduction of one fragment of type k. From the definition of f, one may rewrite Eq. (A9),

$$f_{A,m}(b)=\sum_{k\in b}\omega_k f_{A-a_k,m-1}, \tag{A10}$$

which leads to the recursive expression for F,

$$F_{b,A,m}=\sum_{k\in b}\omega_k F_{b,A-a_k,m-1}\frac{\Omega_{A-a_k}}{\Omega_A}. \tag{A11}$$

This recursion relation allows one to calculate factorial moments of increasing order and for increasingly large nuclei given knowledge of the partition function.

3. Obtaining the multiplicity distribution from the factorial moments

One can express the multiplicity distribution $P_{b,A,n}$ in terms of the factorial moments. Here, $P_{b,A,n}$ is the probability of observing n fragments of type b in an event from a system of mass A. The desired expression, which we derive further below, has the simple form,

$$P_{b,A,n}=\sum_{m\geqslant n}F_{b,A,m}\frac{1}{(m-n)!n!}(-)^{m-n}, \tag{A12}$$

where $F_{b,A,m}=\langle n_b(n_b-1)\cdots(n_b-m+1)\rangle$. Only factorial moments of order n or greater contribute to $P_{b,A,n}$ since events with multiplicity $n_b<m$ do not contribute to $F_{b,A,m}$.

To prove Eq. (A12) we rewrite the right-hand side of Eq. (A12) using the definition of factorial moments

$$\begin{aligned}\sum_{m\geqslant n}F_{b,A,m}\frac{1}{(m-n)!n!}(-)^{m-n}&=\sum_{m\geqslant n}\sum_{l\geqslant m}P_{b,A,l}\frac{l!}{(l-m)!}\frac{1}{(m-n)!n!}(-)^{m-n}\\&=\sum_{l\geqslant n}\sum_{m=0}^{l-n}P_{b,A,l}\frac{l!}{(l-n-m)!}\frac{1}{m!n!}(-)^{m},\end{aligned} \tag{A13}$$

where, in practice, the sums do not extend to ∞ due to the finite size of the system. The sum over m can now be eliminated by using the identity

$$\sum_{m=0}^{k}\frac{k!}{(k-m)!m!}(-)^m=(1-1)^k=\delta_{k,0}, \tag{A14}$$

to obtain Eq. (A12). Although Eq. (A12) is easy to implement numerically, it is susceptible to problems with numerical accuracy due to the alternating signs. Our experience is that such problems set in when the multiplicities approach or exceed 10. However, a recursion relation for the multiplicity distribution, which is derived in the next section, allows calculation of the multiplicity distribution without first calculating the moments. Such an expression does not have alternating signs and therefore is less susceptible to numerical problems.

4. The recursion relation for the multiplicity distribution

In the previous sections of the Appendix, relations have been derived that give a recursion relation for the factorial moments, and also give the multiplicity distribution in terms of the factorial moments. In this section we derive a recursion relation for the multiplicity distribution, that will allow the calculation of the multiplicity distribution without first calculating the moments.

By inserting the recursion relation for factorial moments, Eq. (A11), into the formula for deriving the multiplicity distribution in terms of factorial moments, Eq. (A12), one obtains

$$\begin{aligned}P_{b,A,n}&=\sum_{m\geqslant n}\frac{1}{(m-n)!n!}(-)^{m-n}\sum_{k\in b}\omega_k F_{b,A-a_k,m-1}\frac{\Omega_{A-a_k}}{\Omega_A}\\&=\sum_{k\in b}\omega_k\frac{\Omega_{A-a_k}}{\Omega_A}\sum_{m\geqslant 0}\frac{1}{m!n!}(-)^m F_{b,A-a_k,n+m-1}.\end{aligned} \tag{A15}$$

By replacing $F_{b,A-a_k,n+m-1}$ in the above expression with its definition in terms of the multiplicity distribution

$$\begin{aligned}P_{b,A,n}&=\sum_{k\in b}\omega_k\frac{\Omega_{A-a_k}}{\Omega_A}\sum_{m\geqslant 0}\frac{1}{m!n!}(-)^m\\&\quad\times\sum_{m'\geqslant 0}P_{b,A-a_k,n+m+m'-1}\frac{(n+m+m'-1)!}{m'!)}\\&=\sum_{k\in b}\omega_k\frac{\Omega_{A-a_k}}{\Omega_A}\sum_{M\geqslant 0}P_{b,A-a_k,n+M-1}\frac{(n+M-1)!}{n!}\\&\quad\times\sum_{0\leqslant m\leqslant M}(-)^m\frac{1}{m!(M-m)!}\\&=\sum_{k\in b}\omega_k\frac{\Omega_{A-a_k}}{\Omega_A}P_{b,A-a_k,n-1}\frac{1}{n},\end{aligned} \tag{A16}$$

where the last step utilized the identity, Eq. (A14).

In practice, the multiplicity distributions are calculated for small A, then for successively larger A using the recursion relation above. However, calculation of the $n=0$ term cannot be determined from the recursion relation and must be determined through the constraint $\Sigma_n P_n=1$.

[1] W. Bauer, Phys. Lett. **150B**, 53 (1985); W. Bauer *et al.*, Nucl. Phys. **A452**, 699 (1986); W. Bauer, Phys. Rev. C **38**, 1297 (1986); W. Bauer and A. Botvina, *ibid.* **52**, R1760 (1995).
[2] X. Campi, J. Phys. A **19**, L917 (1986); Phys. Lett. B **208**, 351 (1988).
[3] J. Pan and S. Das Gupta, Phys. Rev. C **51**, 1384 (1995).
[4] W.A. Friedman, Phys. Rev. C **42**, 667 (1990).
[5] P. Chomaz, Ann. Phys. (Paris) **21**, 669 (1996); G.F. Burgio, Ph. Chomaz, and J. Randrup, Phys. Rev. Lett. **69**, 885 (1992).
[6] A. Ohnishi and J. Randrup, Phys. Lett. B **394**, 260 (1997).
[7] H. Feldmeier and J. Schnack, Prog. Part. Nucl. Phys. **39**, 393 (1997).
[8] D. Kiderlen and P. Danielewicz, Nucl. Phys. **A620**, 346 (1997).
[9] S. Pratt, C. Montoya, and F. Ronning, Phys. Lett. B **349**, 261 (1995).
[10] J. Randrup and S.E. Koonin, Nucl. Phys. **A356**, 321 (1981).
[11] S.E. Koonin and J. Randrup, Nucl. Phys. **A474**, 173 (1987).
[12] D.H.E. Gross, Rep. Prog. Phys. **53**, 605 (1990); Phys. Rep. **279**, 119 (1997).
[13] J.P. Bondorf, A.S. Botvina, A.S. Iljinov, I.N. Mishustin, and K. Sneppen, Phys. Rep. **257**, 133 (1995).
[14] L.G. Moretto *et al.*, Phys. Rev. Lett. **74**, 1530 (1995); L.G. Moretto *et al.*, Phys. Rep. **287**, 249 (1997).
[15] J. Toke, D.K. Agnihotri, B. Djerroud, W. Skulski, and W.U. Schroeder, Phys. Rev. C **56**, R1683 (1997).
[16] M.B. Tsang and P. Danielewicz, Phys. Rev. Lett. **80**, 1178 (1998).
[17] W. Bauer and S. Pratt, Report No. nucl-th/9809024, 1998.
[18] L.G. Moretto, L. Bealieu, L. Phair, and G.J. Wozniak, nucl-ex/9709001, 1997.
[19] K.C. Chase and A.Z. Mekjian, Phys. Rev. C **52**, R2339 (1995).
[20] S. Das Gupta and A.Z. Mekjian, Phys. Rev. C **57**, 1361 (1998).
[21] G. Fai and J. Randrup, Nucl. Phys. **A404**, 551 (1983).
[22] A. Bohr and B.R. Mottleson, *Nuclear Structure* (World Scientific, Singapore, 1998), Vol. 1.
[23] S. Pratt, nucl-th/9905055, 1999.
[24] T. Ericson, Adv. Phys. **9**, 425 (1960).
[25] T. Gharib, W. Bauer, and S. Pratt, Phys. Lett. B **444**, 231 (1998).
[26] J.P. Bondorf, A.S. Botvina, and I.N. Mishustin, Phys. Rev. C **58**, R27 (1998).
[27] A. Chbihi, O. Schapiro, D.H.E. Gross, and S. Salou, nucl-th/9901016, 1999.
[28] P. Bhattacharyya, S. Das Gupta, and A.Z. Mekjian, Phys. Rev. C **60**, 054616 (1999).
[29] S.J. Lee and A.Z. Mekjian, Phys. Rev. C **47**, 2266 (1993); **45**, 1284 (1992); **50**, 3025 (1994).